Excitonic giant Zeeman effect in GaN:Mn^{3+}

W. Pacuski,[1,2,*] D. Ferrand,[1,†] J. Cibert,[1] J. A. Gaj,[2] A. Golnik,[2] P. Kossacki,[2] S. Marcet,[1] E. Sarigiannidou,[1,‡] and H. Mariette[1]

[1]*Institut Néel/CNRS, Université J. Fourier, Boîte Postale 166, F-38042 Grenoble Cedex 9, France*

[2]*Institute of Experimental Physics, Warsaw University, Hoża 69, PL-00-681 Warszawa, Poland*

(Received 2 March 2007; revised manuscript received 22 August 2007; published 5 October 2007)

We describe a direct observation of the excitonic giant Zeeman splitting in $Ga_{1-x}Mn_xN$, a wide-gap III-V diluted magnetic semiconductor. Reflectivity and absorption spectra measured at low temperatures display the *A* and *B* excitons, with a shift under magnetic field due to *s*,*p*-*d* exchange interactions. Using an excitonic model, we determine the difference of exchange integrals between Mn^{3+} and free carriers in GaN, $N_0(\alpha-\beta)=-1.2\pm0.2$ eV. Assuming a reasonable value of α, this implies a positive sign of β which corresponds to a rarely observed ferromagnetic interaction between the magnetic ions and the holes involved in the transition.

DOI: 10.1103/PhysRevB.76.165304 PACS number(s): 75.50.Pp, 75.30.Hx, 78.20.Ls, 71.35.Ji

I. INTRODUCTION

Diluted magnetic semiconductors (DMSs) based on III-V compounds, such as (Ga,Mn)As, attract attention mainly because of their magnetic and magnetotransport properties. In these DMSs, due to free carriers introduced by the magnetic ions, the direct measurement of the strength of the ion-carrier coupling through the observation of the giant Zeeman splitting of excitons, as routinely performed in II-VI DMS, is generally not accessible. Hence, conclusions have been based on studies of extremely diluted samples[1] or on a complex interpretation of experimental data.[2–4]

Here, we show and quantitatively describe excitons in GaN, with a shift due to the *s*,*p*-*d* coupling to Mn ions incorporated as neutral centers (Mn^{3+}). We present both the magneto-optical study of especially designed and thoroughly characterized $Ga_{1-x}Mn_xN$ layers and the excitonic model needed to determine the strength of ion-carrier coupling. Such a model is needed, because excitonic effects are especially strong in wide-gap semiconductors. Hence, the giant Zeeman splitting measured on the excitons cannot be identified with that of band-to-band transitions, as it has been done for other wurtzite DMS.[5,6]

II. SAMPLES

$Ga_{1-x}Mn_xN$ layers, about 400 nm thick, were grown by molecular beam epitaxy on sapphire substrates with a GaN or AlN buffer layer, with the *c* axis perpendicular to the surface.[7,8] Layers grown with a GaN buffer allowed us to study quantitatively[9] the infrared absorption identified in quasibulk crystals[10] as due to Mn^{3+} (d^4 ion configuration). These layers exhibit[9] magnetic circular dichroism at the band gap energy, ascribed[11] to the ion-carrier coupling. Layers with a higher Mn content evidence[8] a ferromagnetic behavior at low temperature. The present $Ga_{1-x}Mn_xN$ layers have been grown on a buffer layer made of AlN, which has a large energy gap (E_g over 6 eV), so that the excitonic spectra of $Ga_{1-x}Mn_xN$ (E_g about 3.5 eV) are not entangled with those of the buffer layer. However, the presence of the AlN buffer layer with a lattice mismatch introduces strain and disorder, which increases the excitonic linewidth. As disorder increases also with the Mn content, we focused our study onto rather dilute samples ($x<1.2\%$) exhibiting well-resolved excitons.

The concentration of Mn^{3+} has been determined using near infrared spectroscopy. We observe sharp absorption lines previously reported[9,10] as intraionic $^5T_2 \rightarrow {}^5E$ transitions of Mn^{3+}. The intensity of these lines has been calibrated[9] against secondary ion mass spectrometry (SIMS) in samples, where the d^4 configuration of Mn has been confirmed[12] by x-ray absorption at the Mn *K* edge. In the present series of samples, the intensity of the Mn^{3+} absorption follows the total Mn concentration determined by SIMS with an accuracy better than 10%. Furthermore, a Mn^{2+} concentration lower than 0.01% was deduced from the absence of the characteristic lines in electron paramagnetic resonance (EPR) spectra.[13]

III. EXCITON SPECTROSCOPY

In wurtzite GaN, the crystal field and the spin-orbit coupling split the valence band into three components, from which three excitons are formed, labeled *A*, *B*, and *C* in the order of increasing energy. The valence band ordering is the natural one with band edge *A* of symmetry Γ_9 and band edges *B* and *C* of symmetry Γ_7.[14] The selection rules result in a strong optical anisotropy. For σ polarization (electric field *E* perpendicular to the *c* axis), the oscillator strength is larger for excitons *A* and *B* than for exciton *C*. Exciton *C* has a large oscillator strength in π polarization ($E\|c$). The position and oscillator strength of all excitons, and particularly exciton *C*, are modified by strain.[15]

We measured reflectivity at temperatures down to 1.7 K using a high-pressure Xe lamp, a 0.46 m monochromator, and a charge coupled device camera. In our configuration with light propagating along the *c* axis, only the σ polarization is accessible. In zero-field spectra, we observe two characteristic features. For the most diluted sample [$x=0.01\%$, Fig. 1(a)], the energy of these features corresponds to the energy of the *A* and *B* excitons in GaN, shifted toward high energy by a biaxial compressive strain estimated to be about 19 kbar according to Ref. 15. Such a strain strongly reduces the oscillator strength of exciton *C*. In addition, exciton *C* is

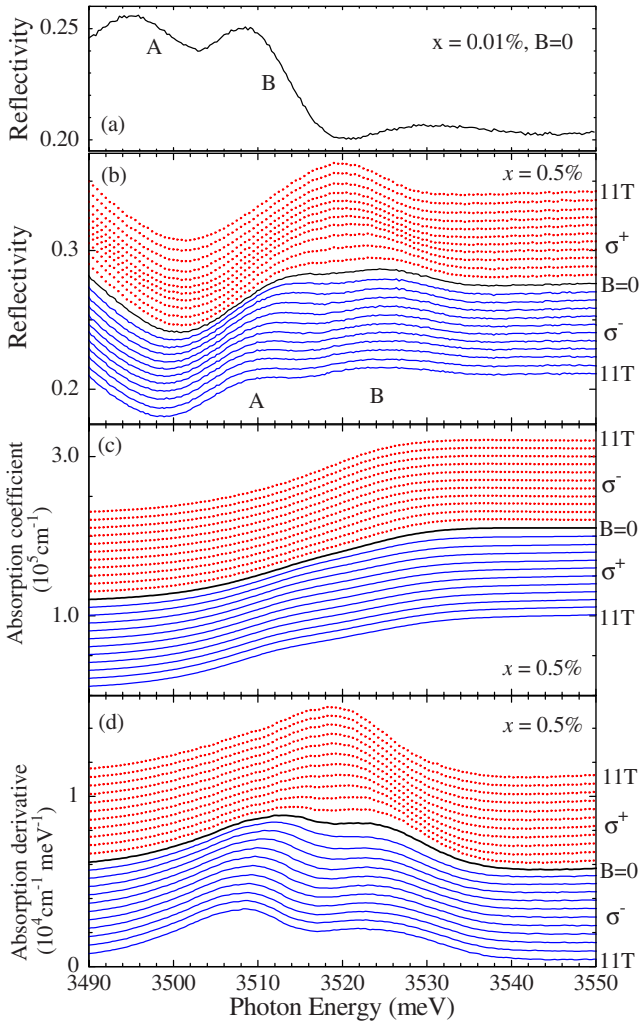

FIG. 1. (Color online) (a) Reflectivity measured for $Ga_{1-x}Mn_xN$ with $x=0.01\%$. (b) Reflectivity, (c) absorption, and (d) derivative of absorption for $x=0.5\%$ in Faraday configuration in σ^+ (red dots) and σ^- (blue solid lines) circular polarizations at $T=1.7$ K. In (b)–(d) spectra are shifted for clarity; the left axis is valid for $B=11$ T in σ^- polarization.

particularly sensitive to broadening due to strain disorder. This explains why we do not observe a third structure at 3540 meV, as expected for exciton *C* for such a strain value. In another sample with $x=0.5\%$ [see the middle spectra marked as $B=0$ in Fig. 1(b)], the *A* and *B* excitonic features are further broadened and shifted to higher energies. This shift confirms the increase of the band gap energy upon increasing the Mn content, previously inferred from magnetic circular dichroism spectra.[9]

Magneto-optical spectra were measured in the Faraday configuration, with the magnetic field parallel to the common *c* axis and optical axis. We recorded reflectivity spectra in both circular polarizations using a quarter wave plate and a linear polarizer and by sweeping the magnetic field from −11 T up to +11 T. The σ^+ and σ^- circular polarizations are defined with respect to the direction of a positive applied field. Magnetoreflectivity spectra of pure GaN or very diluted GaN:Mn ($x=0.01\%$), not shown, exhibit a very small

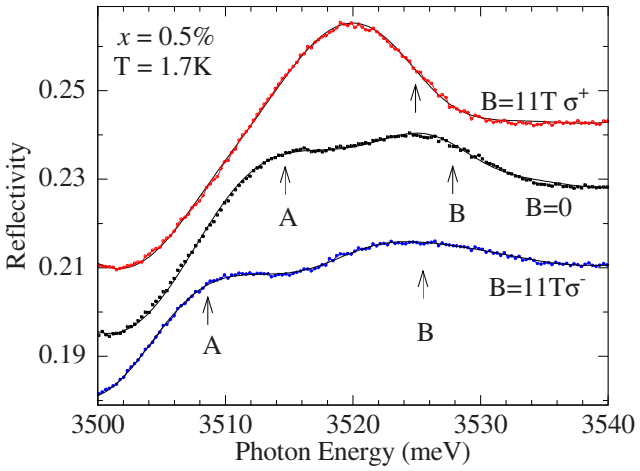

FIG. 2. (Color online) Details of the reflectivity spectra shown in Fig. 1(b) for the sample with $x=0.5\%$ at $T=1.7$ K; experimental spectra are shown by dots and calculated spectra by solid lines. The values of exciton energy used in the calculation and plotted in Fig. 3 (filled circles) are shown by vertical arrows.

excitonic Zeeman shift, $\Delta E<0.5$ meV, even at $B=11$ T, in agreement with previously reported data on GaN.[16,17]

The Zeeman shift of excitons is strongly enhanced in the presence of a significant content of Mn ions. This is shown in Fig. 1(b), which displays reflectivity spectra of the sample with $x=0.5\%$, at 1.7 K and different values of the applied field. Exciton *A* shifts to low energy (redshift) in σ^- polarization ($\Delta E=6$ meV at $B=11$ T). Note that the saturation of the redshift of *A* starts at quite high field values when compared to other DMS containing Mn^{2+} (d^5 configuration). In σ^+, it shifts to high energy and merges with the *B* exciton. The behavior of exciton *B* is more complex. Excitons *A* and *B* are observed also in absorption, Fig. 1(c); however, excitonic features are more visible in the derivative of these absorption spectra, Fig. 1(d), which confirm the observations made on the reflectivity spectra.

The positions of excitonic features were determined by different methods. The most advanced method involves a detailed fit of the reflectivity spectra using a model based on the dielectric function related to the three excitons *A*, *B*, and *C*, including their optically active excited states, and transitions to the continuum of states, as described in Refs. 18 and 19. The dielectric function was calculated for the system formed by the 374 nm thick (Ga,Mn)N layer deposited on a semi-infinite substrate with a refractive index of 1.8. The total reflectivity of the structure was calculated, and therefore, interferences within the thin layer are automatically taken into account. As an example, Fig. 2 displays the fit of experimental spectra recorded in zero field and at 11 T. The values of exciton energy entering this fit are shown by full circles in Fig. 3. A simpler method to determine the field dependence of the exciton energy is based on the determination of a characteristic point in the spectra. We have chosen the maximum of reflectivity and the maximum of the absorption derivative, and these maxima were determined either by visual pointing or by a local fit with two Gaussian lines. All methods give very similar results, as shown by different

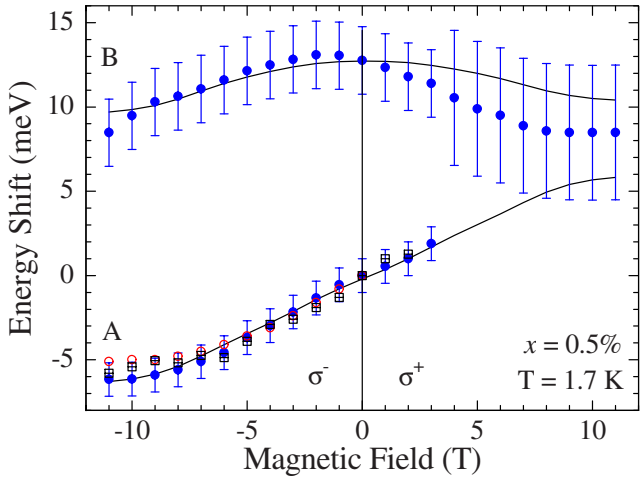

FIG. 3. (Color online) Zeeman shifts of excitonic transitions determined from the fit of reflectivity spectra (filled circles, blue), from the reflectivity maxima (empty squares, black), and from the maxima of absorption derivative (empty circles, red) at $T=1.7$ K and $B\|c$. Corresponding spectra are shown in Figs. 1(b), 1(d), and 2. Solid lines represent the excitonic shifts calculated using the model and with parameters as discussed in the text.

symbols in Fig. 3. In particular, the redshift of exciton A was the same, to within 1 meV, for all methods. We take this value of 1 meV as our experimental accuracy in the determination of the redshift of exciton A. The accuracy in the determination of the position of exciton B is significantly worse, ±2 meV. Finally, in σ^+ polarization at $B>3$ T, excitons A and B merge; therefore, the only feature which remains is marked in Fig. 3 with error bars taken as the value of the A-B splitting for the last resolved spectra. We will come back later on to the redshift of exciton A, which provides us with a particularly easy way of measuring a quantity proportional to the magnetization.

IV. ANALYSIS

We now turn to a detailed analysis of shifts such as observed in Fig. 3. It includes the proper description of the valence band and of excitons in GaN, the strength of the s,p-d exchange interactions, and the magnetic properties of Mn in GaN.

We first briefly note the different components entering the excitonic Hamiltonian and discuss necessary assumptions. In zero field, the energy of a hole in the valence band of a semiconductor with the wurtzite structure is given by[20]

$$H_v = -\tilde{\Delta}_1(L_z^2 - 1) - 2\Delta_2 L_z s_z - 2\Delta_3(L_x s_x + L_y s_y), \quad (1)$$

where $\tilde{\Delta}_1$ describes the effect of the trigonal components of crystal field and biaxial strain; Δ_2 and Δ_3 are the anisotropic spin-orbit interactions; and L_α and s_α are projections of the orbital and spin momenta, respectively. The z direction is parallel to the c axis. We take into account explicitly the averaged biaxial stress in the layer by using an effective crystal field parameter $\tilde{\Delta}_1$.[14] We do not take into account second order terms, which could lower the crystal symmetry and mix excitons of different symmetries, such as alloy effects or random strain. These terms induce mostly a broadening of the excitonic lines and change weakly the averaged energy of A and B excitons. Their main influence could lead to an increase of the oscillator strength of exciton C but the latter is too weak to be analyzed in our case.

Electron-hole interactions within the exciton result in

$$H_{\text{e-h}} = -R^* + 2\gamma \vec{\mathbf{s}}_e \vec{\mathbf{s}}, \quad (2)$$

where R^* is the binding energy, $\vec{\mathbf{s}}_e$ is the electron spin and $\vec{\mathbf{s}}$ the hole spin, and the electron-hole exchange[16,20] is parametrized by the exchange integral γ. A possible difference in the binding energies of the three excitons cannot be distinguished from a change in the values of $\tilde{\Delta}_1$ or Δ_2 above [Eq. (1)].

Both holes and electrons interact with the Mn ions through the so-called s,p-d exchange. In this work, we use the standard form of the s,p-d Hamiltonian ($H_{s,p\text{-}d}=H_{s\text{-}d}+H_{p\text{-}d}$), which only depends on the relative orientation between the carrier spin and the averaged Mn spin $\langle\vec{\mathbf{S}}\rangle$. It reads

$$H_{s\text{-}d} = -xN_0\alpha \vec{\mathbf{s}}_e \cdot \langle\vec{\mathbf{S}}\rangle \quad (3)$$

for electrons and

$$H_{p\text{-}d} = -xN_0\beta \vec{\mathbf{s}} \cdot \langle\vec{\mathbf{S}}\rangle \quad (4)$$

for holes, where α and β are the s,p-d exchange integrals for electrons and holes, respectively. A more complex description of the p-d interaction for the d^4 electronic configuration has been given in Ref. 21, but our experimental precision does not allow us to evidence any effect of the additional terms involving the orbital momentum. The direct influence of the magnetic field on the exciton (usual Zeeman effect and diamagnetic shift) can also be easily implemented in our model,[16,22] but it is small enough to be safely neglected in the present study.

Finally, our Hamiltonian takes the following form:

$$H = E_0 + H_v + H_{\text{e-h}} + H_{sp\text{-}d}, \quad (5)$$

where E_0 is the band gap energy. For a magnetic field parallel to the c axis and light incident along the same direction, we limit ourselves to subspaces containing excitons optically active in σ polarization (excitons of Γ_5 symmetry). The Hamiltonian separates into two independent operators, each acting in one of the two subspaces corresponding, respectively, to excitons active in the σ^+ and σ^- circular polarizations. For σ^+, we use the following basis: $|s\downarrow p^+\uparrow\rangle$ and $|s\uparrow p^+\downarrow\rangle$ (which are identically active in σ^+ polarization and will give the main contribution to excitons A and B) and $|s\uparrow p^z\uparrow\rangle$ (which is optically inactive since it is spin forbidden but will give the main contribution to exciton C in σ polarization). The arrows denote sign of spin projection of electron (s) and hole (p), respectively. We denote p^+, p^-, and p^z the hole states with orbital momenta +1, −1, and 0, respectively. For σ^- polarization, we use the basis $|s\uparrow p^-\downarrow\rangle$, $|s\downarrow p^-\uparrow\rangle$, and $|s\downarrow p^z\downarrow\rangle$. In these bases, the Hamiltonians are written as[20,23,24]

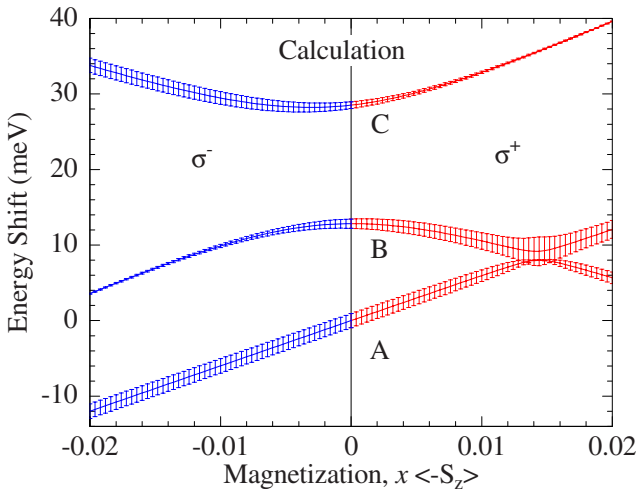

FIG. 4. (Color online) Calculated energy of the A, B, and C excitons vs magnetization expressed as $x\langle -S_z\rangle$ for σ^- (left half) and σ^+ (right half) circular polarizations. Oscillator strengths are shown by bars.

$$H_v = \begin{pmatrix} -\Delta_2 & 0 & 0 \\ 0 & \Delta_2 & -\sqrt{2}\Delta_3 \\ 0 & -\sqrt{2}\Delta_3 & \tilde{\Delta}_1 \end{pmatrix}, \tag{6}$$

$$H_{\text{e-h}} = -R^* + \frac{\gamma}{2}\begin{pmatrix} -1 & 2 & 0 \\ 2 & -1 & 0 \\ 0 & 0 & 1 \end{pmatrix}, \tag{7}$$

$$H_{sp\text{-}d}^{\sigma\pm} = \pm\frac{1}{2}N_0 x\langle -S_z\rangle\begin{pmatrix} \beta-\alpha & 0 & 0 \\ 0 & \alpha-\beta & 0 \\ 0 & 0 & \alpha+\beta \end{pmatrix}. \tag{8}$$

The only difference between the matrices for σ^+ and σ^- polarizations is the opposite sign of the giant Zeeman term. We do not give the corresponding matrices for the other six excitons (of symmetries Γ_1, Γ_2, and Γ_6), which are not optically active in σ polarizations.

Diagonalizing the Hamiltonian gives the energy of the three excitons A, B, and C in each circular polarization, as plotted in Fig. 4. The corresponding oscillator strength is deduced from the projection of the eigenvector $|\psi\rangle$ onto the relevant subspace active in circular polarization: it is proportional to $|\langle s\downarrow p^{\pm}\uparrow|\psi\rangle + \langle s\uparrow p^{\pm}\downarrow|\psi\rangle|^2$ for $\sigma^{\pm}$ circular polarization, respectively. It is marked by bars ib Fig. 4.

We use the excitonic model described above to fit the experimental data shown in Fig. 3. The fitting parameters were determined as follows: we use $\Delta_3 = 5.5$ meV and $\gamma = 0.6$ meV as reported for pure GaN, (Refs. 15 and 20) and calculate the mean spin of Mn^{3+} $\langle -S_z\rangle$ from the expression given in Ref. 9. Finally, we fit the data by keeping $\tilde{\Delta}_1$, Δ_2, and $N_0(\alpha-\beta)$ as free parameters. The best fit was obtained with $\tilde{\Delta}_1 = 11$ meV and $\Delta_2 = 10$ meV, and we determine $N_0(\alpha-\beta) = -1.2\pm0.2$ eV.

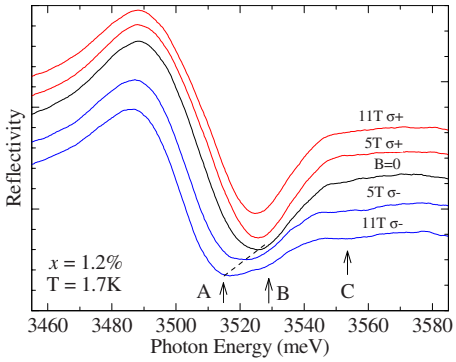

FIG. 5. (Color online) Reflectivity of the sample with the highest Mn concentration ($x = 1.2\%$). Due to the increase of the linewidths, excitons A and B are not resolved in zero field and in σ^+ polarization. Nevertheless, the giant Zeeman effect can be clearly observed by the redshift of exciton A in σ^- polarization (the dashed line is a guide for the eye). In the same polarization, the blueshift of exciton B increases the mixing between excitons B and C, so that exciton C can be observed at high field.

In zero field, the relative position of the excitons is determined mainly by the trigonal component of the crystal field including strain $\tilde{\Delta}_1$ and the parallel spin-orbit interaction Δ_2. The giant Zeeman shift of the excitons is induced by $s,p\text{-}d$ interactions. It leads to crossings of exciton A with B and of B with C. The electron-hole exchange interaction γ governs the anticrossing and mixing of the A and B excitons. It strongly alters the excitonic oscillator strength. The perpendicular spin-orbit interaction (Δ_3) is responsible for the anticrossing and mixing between the B and C excitons. The giant Zeeman shift of exciton A is governed by $N_0(\alpha-\beta)$ and quite insensitive to the exact value of $N_0\alpha$; in order to plot Fig. 4, we used $N_0\alpha = 0.2$ eV, the usual value reported in II-VI DMSs. In practice, the value $N_0(\alpha-\beta) = -1.2\pm0.2$ eV, obtained from the fit above, can be read directly on the slope of exciton A in σ^- polarization. The latter method will be used for a whole series of samples below.

The separate determination of $N_0\alpha$ and $N_0\beta$ would require fitting the giant Zeeman shift of exciton C, which is governed by $N_0(\alpha+\beta)$, or having a stronger anticrossing between excitons B and C at high field (i.e., higher Mn concentration or smaller $\tilde{\Delta}_1$). An example of spectra on a sample with a larger Mn content is shown in Fig. 5. The Zeeman shift of exciton B in σ^- polarization increases significantly the mixing with exciton C. As a result, at high field, exciton C acquires an oscillator strength sufficient to be observed. This is in good qualitative agreement with the predictions of the exciton model, but the linewidth is too large and precludes any quantitative study.

An important result is that, generally speaking, the giant Zeeman splitting of excitons A and B is not proportional to the Mn magnetization. In order to probe the giant Zeeman energy $[N_0(\alpha-\beta)x\langle -S_z\rangle]$, one should rather use the redshift of exciton A in σ^- polarization, which appears to be proportional to the magnetization as shown by the straight line in Fig. 4. This redshift of A is well accounted for over a large range of fields and temperatures, as shown in Fig. 6(a),

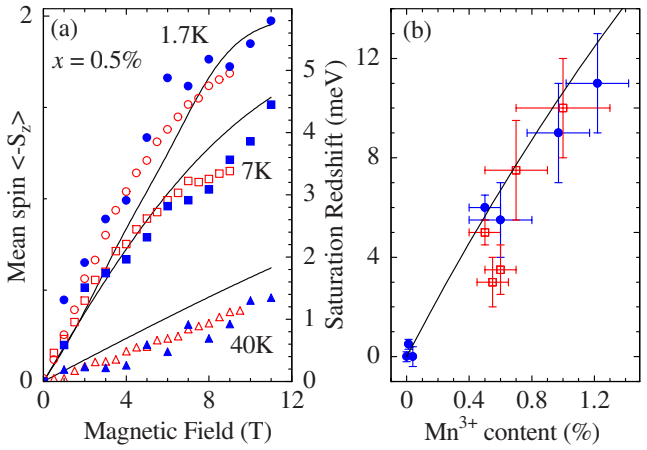

FIG. 6. (Color online) (a) Redshift of exciton A determined using reflectivity (full symbols, blue) and absorption (empty symbols, red) compared to the mean spin of Mn^{3+} (solid lines, right axis) calculated using Ref. 9, for temperatures 1.7, 7, and 40 K. (b) Giant Zeeman shift of exciton A at saturation determined using reflectivity (full circles, blue) and absorption (empty squares, red). Solid line represents value of the shift $\Delta E_A=-(1/2)N_0(\alpha-\beta)\times x_{\text{eff}}\langle -S_z\rangle$ calculated with $N_0(\alpha-\beta)=-1.2$ eV, $\langle -S_z\rangle=2$, and $x_{\text{eff}}=x(1-x)$ (Ref. 12).

where the mean spin of Mn^{3+} is calculated using Ref. 9. Both saturate only at the lowest temperature and highest magnetic field, in agreement with the fact that the field is applied along the hard magnetization axis of the strongly anisotropic Mn^{3+} ion. Any contribution from Mn^{2+} ions would saturate at low field (3 T), as does the Brillouin function for d^5. From the data presented in Fig. 6(a), we conclude that such a contribution should be at least 1 order of magnitude weaker than the Mn^{3+} contribution. This agrees with the negligible Mn^{2+} content ($x<0.01\%$) estimated by EPR[13] on the same sample, compared to the Mn^{3+} content equal to $x=0.5\%$, determined from d-d absorption.

This magneto-optical study was extended to a whole series of samples [see Fig. 6(b)]. We performed a detailed analysis of A and B excitons by fitting the A and B excitonic energies only for the diluted samples. For higher Mn concentrations, the behavior of A and B excitons under magnetic field is qualitatively similar (see Fig. 5), but the line broadening prevents any precise fit of the spectra. Nevertheless, the giant Zeeman effect can be unambiguously determined using the Zeeman shift of exciton A in σ^- polarization. As expected, it increases with the Mn^{3+} content determined from d-d absorption. In Fig. 6(b), it is compared, as usual, to the effective concentration $x_{\text{eff}}=x(1-x)$,[12] rather than to the total concentration x, which accounts for the small nonlinear variation of the redshift. x_{eff} corresponds to the density of Mn impurities with no magnetic ion over the 12 nearest neighbors present in the Ga sublattice[25] and is used to take into account an antiferromagnetic blocking of the Mn-Mn nearest neighbor pairs at low temperature. As shown in Fig. 6(b), the value $N_0(\alpha-\beta)=-1.2\pm0.2$ eV determined previously accounts well for the giant Zeeman effect observed in the whole concentration range. We can note that a spin splitting of exciton A of about 20 meV can be obtained with a Mn concentration of about 1%.

V. DISCUSSION

The redshift of exciton A in σ^- polarization unambiguously points to a negative sign of $N_0(\alpha-\beta)$. So far, $|N_0\alpha|$ has been reported to be small (<0.3 eV) and almost constant for all DMSs, and there is no theoretical hint that the case of GaN-based DMS could be different. Then, $N_0(\alpha-\beta)=-1.2$ eV means that β is positive for GaN:Mn^{3+}. If we assume a usual value, $N_0\alpha=0.2\pm0.1$ eV, we deduce $N_0\beta=+1.4\pm0.3$ eV, which means a ferromagnetic interaction between the magnetic ions and the holes.

A positive β was rarely observed in DMS. A known exception[26,27] is Cr in II-VI DMS, where Cr has the same $3d^4$ electronic configuration as Mn^{3+} in GaN. This could suggest that a less than a half-filled d shell would be responsible for a positive β. However, this analogy is probably misleading, because it is essentially the position of the donor and acceptor levels which governs the sign of β (Refs. 21 and 28).

A large negative value of $N_0\beta$ has been deduced from photoemission experiments[4] on (Ga,Mn)N layers where Mn has been observed to be in the 2+ configuration. In our samples, the present magneto-optical observation of the d^4 electronic configuration of Mn in GaN is consistent with x-ray absorption near edge spectroscopy measurements performed at the K edge,[12] infrared absorption,[9,10] magnetic anisotropy,[29] and EPR.[13] It would be interesting to understand whether the different electronic configurations originate from an observation of different samples with different Fermi levels or a sensitivity to different parts of the samples (high sensitivity to the surface in the case of photoemission).

Another explanation could be that our determination of the p-d exchange energy by magneto-optical spectroscopy, considered up to now to be a direct experimental determination of the spin-carrier exchange, and the expectation deduced from the knowledge of the p-d hybridization and the positions of Mn levels, supported by x-ray spectroscopy, actually deal with different quantities. Indeed, it has been recently suggested that in wide band gap DMS, a strong coupling between the band hole and the localized magnetic impurities could reduce and reverse the sign of the giant Zeeman splitting determined optically.[22,30] In that case, the exchange interactions between Mn spins and free holes would be characterized by an apparent and positive exchange integral β^{app}, significantly reduced with respect to the intrinsic, negative value of β, in agreement with the present results.

VI. CONCLUSION

To sum up, the giant Zeeman effect of the A and B excitons has been observed by reflectivity and absorption on a series of $Ga_{1-x}Mn_xN$ samples. It is well described using an excitonic model valid for a DMS with the wurtzite structure and values of the s,p-d exchange integrals such that $N_0(\alpha-\beta)=-1.2\pm0.2$ eV. Assuming a reasonable value of α, we find a positive sign of β, which means that in GaN, the effective interaction between the Mn^{3+} spins and the holes involved in the excitonic transition is ferromagnetic.

ACKNOWLEDGMENTS

We thank P. Sati and A. Stepanov for valuable EPR data. We acknowledge helpful discussions with W. Bardyszewski, T. Dietl, and P. Kacman. The work done in Grenoble was carried out in the CNRS-CEA-UJF Joint Group "Nanophysique et semiconducteurs." This work was partially supported by the Polish Committee for Scientific Research (Grants No. N202 006 31/0153 and No. N202 123 31/1953) and by the French Ministry of Foreign Affairs.

*wojciech.pacuski@fuw.edu.pl
†david.ferrand@grenoble.cnrs.fr
‡Permanent address: LMGP, BP 257, INPGrenoble Minatec, 3 parvis Louis Néel, 38016 Grenoble, France.

[1] R. C. Myers, M. Poggio, N. P. Stern, A. C. Gossard, and D. D. Awschalom, Phys. Rev. Lett. **95**, 017204 (2005).
[2] J. Szczytko, W. Mac, A. Twardowski, F. Matsukura, and H. Ohno, Phys. Rev. B **59**, 12935 (1999).
[3] J. Okabayashi, A. Kimura, O. Rader, T. Mizokawa, A. Fujimori, T. Hayashi, and M. Tanaka, Phys. Rev. B **58**, R4211 (1998).
[4] J. I. Hwang, Y. Ishida, M. Kobayashi, H. Hirata, K. Takubo, T. Mizokawa, A. Fujimori, J. Okamoto, K. Mamiya, Y. Saito, Y. Muramatsu, H. Ott, A. Tanaka, T. Kondo, and H. Munekata, Phys. Rev. B **72**, 085216 (2005).
[5] R. L. Aggarwal, S. N. Jasperson, J. Stankiewicz, Y. Shapira, S. Foner, B. Khazai, and A. Wold, Phys. Rev. B **28**, 6907 (1983).
[6] M. Arciszewska and M. Nawrocki, J. Phys. Chem. Solids **47**, 309 (1986).
[7] S. Kuroda, E. Bellet-Amalric, R. Giraud, S. Marcet, J. Cibert, and H. Mariette, Appl. Phys. Lett. **83**, 4580 (2003).
[8] E. Sarigiannidou, F. Wilhelm, E. Monroy, R. M. Galera, E. Bellet-Amalric, A. Rogalev, J. Goulon, J. Cibert, and H. Mariette, Phys. Rev. B **74**, 041306(R) (2006).
[9] S. Marcet, D. Ferrand, D. Halley, S. Kuroda, H. Mariette, E. Gheeraert, F. J. Teran, M. L. Sadowski, R. M. Galera, and J. Cibert, Phys. Rev. B **74**, 125201 (2006).
[10] A. Wołos, A. Wysmolek, M. Kaminska, A. Twardowski, M. Bockowski, I. Grzegory, S. Porowski, and M. Potemski, Phys. Rev. B **70**, 245202 (2004).
[11] K. Ando, Appl. Phys. Lett. **82**, 100 (2003).
[12] A. Titov, X. Biquard, D. Halley, S. Kuroda, E. Bellet-Amalric, H. Mariette, J. Cibert, A. E. Merad, G. Merad, M. B. Kanoun, E. Kulatov, and Yu. A. Uspenskii, Phys. Rev. B **72**, 115209 (2005).
[13] P. Sati and A. Stepanov (private communication).
[14] B. Gil and O. Briot, Phys. Rev. B **55**, 2530 (1997).
[15] B. Gil, O. Briot, and R. L. Aulombard, Phys. Rev. B **52**, R17028 (1995).
[16] R. Stępniewski, M. Potemski, A. Wysmołek, K. Pakuła, J. M. Baranowski, J. Łusakowski, I. Grzegory, S. Porowski, G. Martinez, and P. Wyder, Phys. Rev. B **60**, 4438 (1999).
[17] J. Campo, M. Julier, D. Coquillat, J. P. Lascaray, D. Scalbert, and O. Briot, Phys. Rev. B **56**, R7108 (1997).
[18] C. Tanguy, Phys. Rev. Lett. **75**, 4090 (1995).
[19] A. Golnik, W. Mac, K. Pakula, R. Stepniewski, C. Testelin, and J. Gaj, Solid State Commun. **124**, 89 (2002).
[20] M. Julier, J. Campo, B. Gil, J. P. Lascaray, and S. Nakamura, Phys. Rev. B **57**, R6791 (1998).
[21] A. K. Bhattacharjee, Phys. Rev. B **49**, 13987 (1994).
[22] W. Pacuski, P. Kossacki, D. Ferrand, A. Golnik, J. Cibert, M. Wegscheider, A. Navarro-Quezada, A. Bonanni, M. Kiecana, M. Sawicki, and T. Dietl, arXiv:0708.3296 (unpublished).
[23] W. Pacuski, D. Ferrand, J. Cibert, C. Deparis, J. A. Gaj, P. Kossacki, and C. Morhain, Phys. Rev. B **73**, 035214 (2006).
[24] W. Pacuski, D. Ferrand, P. Kossacki, S. Marcet, J. Cibert, J. A. Gaj, and A. Golnik, Acta Phys. Pol. A **110**, 303 (2006).
[25] Y. Shapira, S. Foner, D. H. Ridgley, K. Dwight, and A. Wold, Phys. Rev. B **30**, 4021 (1984).
[26] W. Mac, N. T. Khoi, A. Twardowski, J. A. Gaj, and M. Demianiuk, Phys. Rev. Lett. **71**, 2327 (1993).
[27] M. Herbich, W. Mac, A. Twardowski, K. Ando, Y. Shapira, and M. Demianiuk, Phys. Rev. B **58**, 1912 (1998).
[28] J. Blinowski and P. Kacman, Acta Phys. Pol. A **100**, 343 (2001).
[29] J. Gosk, M. Zajac, A. Wołos, M. Kaminska, A. Twardowski, I. Grzegory, M. Bockowski, and S. Porowski, Phys. Rev. B **71**, 094432 (2005).
[30] T. Dietl, arXiv:cond-mat/0703278 (unpublished).